RESEARCH ARTICLE | OCTOBER 28 2025

Effects of initial spin orientation on the generation of polarized electron beams from laser wakefield acceleration in plasma

L. R. Yin 1; X. F. Li $\overset{\blacksquare}{\blacksquare}$ 0; Y. J. Gu $\overset{\blacksquare}{\blacksquare}$; N. Cao; Q. Kong $\overset{\blacksquare}{\blacksquare}$; M. Büscher $\overset{\blacksquare}{\blacksquare}$; S. M. Weng $\overset{\blacksquare}{\blacksquare}$; M. Chen $\overset{\blacksquare}{\blacksquare}$; Z. M. Sheng $\overset{\blacksquare}{\blacksquare}$



Matter Radiat. Extremes 11, 017202 (2026) https://doi.org/10.1063/5.0279175





Articles You May Be Interested In

On the spin-quantization-axis selection for the spin polarization modeling during laser-electron collision

Phys. Plasmas (February 2024)

Enhanced MVA of polarized proton beams via PW laser-driven plasma bubble

Matter Radiat. Extremes (April 2025)

Spin-polarized electron beam generation in the colliding-pulse injection scheme

Matter Radiat. Extremes (October 2023)





Effects of initial spin orientation on the generation of polarized electron beams from laser wakefield acceleration in plasma

Cite as: Matter Radiat. Extremes 11, 017202 (2026); doi: 10.1063/5.0279175 Submitted: 6 May 2025 • Accepted: 10 October 2025 •







Published Online: 28 October 2025

L. R. Yin,¹ D X. F. Li,^{2,a)} D Y. J. Gu,³ N. Cao,⁴ Q. Kong,^{1,b)} M. Büscher,^{5,6} S. M. Weng,^{7,8} M. Chen,^{7,8}





and Z. M. Sheng^{7,8,9}

AFFILIATIONS

- 1 Key Laboratory of Nuclear Physics and Ion-Beam Application (MoE), Institute of Modern Physics, Department of Nuclear Science and Technology, Fudan University, Shanghai 200433, China
- ²State Key Laboratory of Ultra-intense Laser Science and Technology, Shanghai Institute of Optics and Fine Mechanics, Chinese Academy of Sciences, Shanghai 201800, China
- SANKEN (Institute of Scientific and Industrial Research), Osaka University, Mihogaoka 8-1, Ibaraki, Osaka 567-0047, Japan
- Sichuan Research Institute, Shanghai Jiao Tong University, Chengdu, Sichuan 610200, China
- ⁵Peter Grünberg Institut (PGI-6), Forschungszentrum Jülich, Wilhelm-Johnen-Str. 1, 52425 Jülich, Germany
- ⁶Institut für Laser-und Plasmaphysik, Heinrich-Heine-Universität Düsseldorf, Universitätsstr. 1, 40225 Düsseldorf, Germany
- Key Laboratory for Laser Plasmas (MoE), School of Physics and Astronomy, Shanghai Jiao Tong University, Shanghai 200240, China
- Collaborative Innovation Center of IFSA, Shanghai Jiao Tong University, Shanghai 200240, China
- ⁹Tsung-Dao Lee Institute, Shanghai Jiao Tong University, Shanghai 200240, China
- a) Author to whom correspondence should be addressed: xiaofengli@siom.ac.cn
- b) Electronic mail: qkong@fudan.edu.cn

ABSTRACT

The effects of initial spin orientation on the final electron beam polarization in laser wakefield acceleration in a pre-polarized plasma are investigated theoretically and numerically. From the results of variation of the initial spin direction, the spin dynamics of the electron beam are found to depend on the self-injection mechanism. The effects of wakefields and laser fields are studied using test particle dynamics and particle-in-cell simulations based on the Thomas-Bargmann-Michel-Telegdi equation. Compared with transverse injection, longitudinal injection is found to be preferable for obtaining a highly polarized electron beam.

© 2025 Author(s). All article content, except where otherwise noted, is licensed under a Creative Commons Attribution (CC BY) license (https://creativecommons.org/licenses/by/4.0/). https://doi.org/10.1063/5.0279175

I. INTRODUCTION

Spin-polarized electron beams have notable applications in nuclear and particle physics as well as high energy physics, 1-10 such as testing the Standard Model of particle physics,^{2,3} exploring the structure of subatomic particles,4 detecting nuclear spin structures,⁵ producing polarized gamma rays and positrons,⁶⁻⁹ and diagnosing characteristics of ultrafast ultraintense laser pulses.¹⁰ In conventional accelerators, such as electron storage rings, the Sokolov-Ternov effect requires approximately several hours to establish polarization. 11,12 On the other hand, conventional electron

accelerators are limited by the breakdown of radio-frequency cavities (100 MV/m) and are large in size, as well as expensive. 13,14 Owing to its extremely high accelerating gradients above 100 GV/m, allowing the acceleration process to be accomplished within a few picoseconds, laser-wakefield acceleration (LWFA) has attracted growing attention. 15,16

Extensive theoretical and experimental investigations of ²⁵ together with the development of pre-polarized plasma targets, 26,27 have led to considerable interest in the possibility of generating spin-polarized electron beams with high-quality via different injection mechanisms. 28-36 Wen et al. 28 proposed that

high-current polarized electron beams could be produced through density-transition injection in a pre-polarized gas plasma generated by laser-induced photodissociation. Wu *et al.*^{29–31} demonstrated that highly spin-polarized electron beams could be obtained by using vortex Laguerre–Gaussian lasers. Nie *et al.*^{32,33} proposed to generate electron beams with high polarization on the basis of the ionization-induced injection mechanism. Recently, it has been proposed that attosecond electron bunches with high spin-polarization could be obtained by using a radially polarized laser.³⁴ It has also been proposed that the colliding-pulse injection mechanism could enable the production of quasi-monoenergetic polarized electron beams using commercial 10 TW laser systems with a pre-polarized plasma.^{35,36}

Among the above studies, particular attention has been paid to the self-injection mechanism, since it is straightforward and is rather easy to implement experimentally. According to the different electron trajectories, the self-injection process is divided into transverse injection and longitudinal injection.³⁷ When an ultra-intense laser pulse propagates into an underdense plasma, electrons near the laser axis are pushed sideways and form a blowout regime behind the laser. Some electrons can be accelerated after they are captured in the tail of the bubble. ¹⁶ In the transverse case, the trapped electrons are initially located at the transverse radii of the bubble fields.³⁹ In the longitudinal case, which mainly occurs in the quasi-1D regime, the captured electrons are initially located near the laser axis, ⁴⁰ and their spins are mainly affected by the laser fields.⁴¹

In the experimental scheme suggested in Ref. 42, the prepolarized plasma is formed by a dedicated laser beam, and it is difficult to perfectly align this with the accelerating laser. Therefore, the electron spin direction forms an angle with the laser axis. In this paper, this phenomenon is investigated, taking into account both the bubble field and laser field. The theoretical analysis is outlined in Sec. II. Numerical simulation results are presented in Sec. III, where transverse and longitudinal self-injections are discussed. Conclusions are given in Sec. IV.

II. THEORETICAL ANALYSIS

The electron spin can be treated as a quasi-classical state with a unit vector s, which has an absolute value of 1. If an electron with velocity v moves in an electromagnetic field, the precession of its spin vector s can be calculated through the Thomas-Bargmann-Michel-Telegdi (TBMT) equation 12,43

$$\frac{\mathrm{d}s}{\mathrm{d}t} = \mathbf{\Omega} \times s,\tag{1}$$

with the spin precession frequency

$$\Omega = \frac{e}{m_e} \left[\left(a_e + \frac{1}{\gamma} \right) \mathbf{B} - \frac{a_e \gamma}{\gamma + 1} \mathbf{v} \cdot \mathbf{B} \frac{\mathbf{v}}{c^2} - \left(a_e + \frac{1}{\gamma + 1} \right) \frac{\mathbf{v}}{c^2} \times \mathbf{E} \right]. \quad (2)$$

Here, m_e , e, and γ are the mass, charge, and Lorentz factor of the electron, $a_e \approx 1.16 \times 10^{-3}$ is the dimensionless anomalous magnetic moment, c is the speed of light in vacuum, B is the magnetic field, and E is the electric field in the laboratory frame. During LWFA,

the radiation reaction, the Stern-Gerlach and the Sokolov-Ternov effects can be ignored according to Ref. 44.

For simplicity, the initial degree of polarization in the plasma is assumed to be 100%, since the effect of the initial spin direction is the main focus of this study. As presented in Fig. 1, a laser with linear polarization along the y direction propagates in the plasma along the x direction. In the general case, the electron spin direction is defined by the pre-polarization angle θ_0 with respect to the x direction and the azimuthal angle β_0 with respect to the y direction, as indicated in Fig. 1. The initial electron spin vector \mathbf{s}_0 can thus be written as $\mathbf{s}_0 = \cos\theta_0\mathbf{i} + \cos\beta_0\sin\theta_0\mathbf{j} + \sin\beta_0\sin\theta_0\mathbf{k}$, as indicated by the yellow arrows in Fig. 1.

When electrons are captured and accelerated in the blowout regime, their depolarization occurs mainly in the injection process rather than the acceleration process. In the case of transverse injection, the precession of electron spin is mainly divided into two stages for the injection process, according to Ref. 39. In the first stage, the electrons arrive at the bubble sheath in the transverse direction, and their spins are affected mainly by the magnetic field B_{φ} and electric field E_r . In the second stage, the electrons are located at the tail of the bubble, and their spins are affected mainly by the electric field E_x . This results in a spin precession frequency of electrons $\Omega \approx \Omega_{\varphi}$, according to Eq. (1), with a constant direction of Ω during the injection process. Cylindrical coordinates, with polar angle φ , are used here because the electromagnetic field is approximately axially symmetric in the bubble regime.

According to Eq. (1), the precession of electron spin is described as rotational motion of the spin vector \mathbf{s} around the direction of the precession frequency Ω . Since the direction of Ω does not change with time, the spin rotation depends on the strength of Ω , and the rotational motion defines the plane AOC, as displayed in Fig. 2. The red and blue arrows represent the initial spin vector $\mathbf{s}_0 = s_{0\psi}\hat{\psi} + s_{0\kappa}\hat{\mathbf{k}}$ and final spin vector $\mathbf{s}_t = s_{t\psi}\hat{\psi} + s_{t\kappa}\hat{\mathbf{k}}$, where $\hat{\psi}$ and $\hat{\mathbf{k}}$ are unit vectors respectively parallel and perpendicular to the direction of Ω . The rotation angle in the rotation plane between the initial state (PA) and final time (PC) is defined as α_r . Therefore, the component of the final spin \mathbf{s}_t along the direction of initial spin \mathbf{s}_0 for an electron can be written as

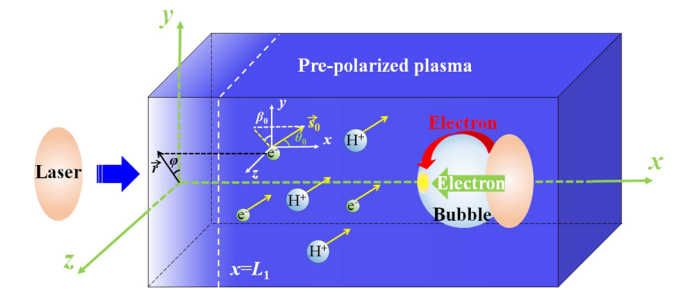


FIG. 1. Schematic of the interaction of laser and pre-polarized plasma. The longitudinal profile of the plasma density consists of a transition from 0 to n_0 with length L_1 and a plateau with n_0 . The laser is focused at the left-hand boundary of the plasma. The initial spin state is defined by the angles θ_0 and β_0 , and is indicated by the yellow arrows. φ denotes the polar angle of a cylindrical coordinate system. The self-injection mechanism for accelerating electrons is divided into transverse (red arrow) and longitudinal (green arrow) schemes according to their trajectories.

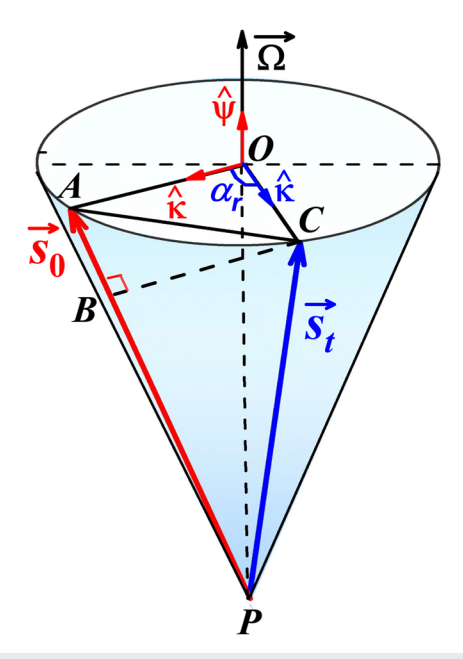


FIG. 2. Schematic of electron spin evolution with a fixed direction of precession frequency Ω . The electron spins at the initial time (\mathbf{s}_0) and final time (\mathbf{s}_t) are denoted by the red and blue arrows, respectively. α_r denotes the rotation angle during Δt in the AOC plane.

$$s_{\parallel} = \mathbf{s}_t \cdot \hat{\mathbf{s}}_0 = 1 - 2|s_{0\kappa}\hat{\mathbf{\kappa}}|^2 \sin^2\left(\frac{\alpha_r}{2}\right). \tag{3}$$

For the accelerated electrons in the bubble field, considering that $\Omega \approx \Omega_{\varphi}$, the component of the initial spin vector \mathbf{s}_0 along $\hat{\boldsymbol{\psi}}$ can be written as

$$|s_{0\psi}\hat{\psi}| = |s_0 \cdot \hat{\varphi}|$$

$$= |(\cos \theta_0 \mathbf{i} + \cos \beta_0 \sin \theta_0 \mathbf{j} + \sin \beta_0 \sin \theta_0 \mathbf{k}) \cdot \hat{\varphi}|$$

$$= |-\sin \theta_0 \cos \beta_0 \sin \varphi + \sin \theta_0 \sin \beta_0 \cos \varphi|. \tag{4}$$

Considering that $|s_{0\kappa}| = \sqrt{1 - |s_{0\psi}|^2}$, Eq. (3) can be rewritten as

$$s_{\parallel} = \cos \alpha_r + \sin^2 \left(\frac{\alpha_r}{2}\right) \sin^2 \theta_0 \left(\sin \beta_0 \cos \varphi - \cos \beta_0 \sin \varphi\right)^2.$$
 (5)

It can be seen that s_{\parallel} is related to the initial polarization direction, i.e., the pre-polarization angle θ_0 and azimuthal angle β_0 , and s_{\parallel} also depends on the electron position and the electromagnetic field, as represented by φ and α_r .

The polarization of the accelerated beam can be derived as the average value of the injected electron spins. In the case of transverse injection, the electrons are initially located in the region around the transverse radius, from $R_{0\,\mathrm{min}}$ to $R_{0\,\mathrm{max}}$. Electrons located at the same distance r from the laser axis are injected into the bubble at the same time. According to Eq. (5), the polarization of the injected electrons can be derived as

$$\langle s_{\parallel} \rangle = \frac{\int_{R_{0 \min}}^{R_{0 \max}} \int_{-\pi}^{\pi} s_{\parallel} r \, d\varphi \, dr}{\int_{R_{0 \min}}^{R_{0 \max}} \int_{-\pi}^{\pi} r \, d\varphi \, dr} = \frac{1}{2} [(\cos \alpha_r)(2 - \sin^2 \theta_0) + \sin^2 \theta_0], \quad (6)$$

where $\langle\cos\alpha_r\rangle=\int_{R_{0\,\mathrm{min}}}^{R_{0\,\mathrm{max}}}\cos\alpha_r\cdot r\;\mathrm{d}r/(R_{0\,\mathrm{max}}^2-R_{0\,\mathrm{min}}^2)$. It should be noted that the value of $\langle s_\parallel\rangle$ depends on θ_0 . However, it is independent of β_0 , which can be always set to zero through a coordinate transformation. Besides, in the case of $\theta_0=0^\circ$, $\langle s_\parallel\rangle=\cos\alpha_r\in[-1,1]$, while in the case of $\theta_0=90^\circ$, $\langle s_\parallel\rangle=\frac{1}{2}(1+\cos\alpha_r)\in[0,1]$. More importantly, the electron polarization $\langle s_\parallel\rangle$ increases monotonically with θ_0 in the range $[0,\pi/2]$, which indicates that the initial state of the electron spin can affect the final polarization.

III. SIMULATION METHODS AND DISCUSSION

To confirm the above theoretical analysis, the electron spin motion is also examined using test particle dynamics and particle-in-cell (PIC) simulations. The PIC simulations are performed with a modified version of the EPOCH code, 45 which includes the spin evolution module based on the TBMT equation via the Boris pusher method. 46 The laser propagates in the x direction with linear polarization along the y direction and a transverse Gaussian envelope

$$E_{y} = \frac{E_{0}w_{0}}{w(x)} \exp \left[-\frac{y^{2} + z^{2}}{w(x)^{2}} - \frac{(t - \tau)^{2}}{(0.5\tau)^{2}} \right] \cos \varphi, \tag{7}$$

where the laser wavelength $\lambda = 800$ nm, $w(x) = w_0 \left[1 + (x - x_0)^2/z_R^2\right]^{1/2}$, $z_R = \pi w_0^2/\lambda$, τ is the laser pulse duration, and $a_0 = eE_0/m_ewc$ is the normalized laser amplitude. The laser pulse is focused at the left edge of the plasma target $(x_0 = 30\lambda)$. The initial longitudinal profile of the pre-polarized plasma is an up-ramp followed by a plateau, 40 as presented in Fig. 1. The normalized laser amplitude a_0 , the spot size w_0 , the length of up-ramp transition L_1 , and the plasma density n_0 are different in the cases of transverse and longitudinal injection. The 2D simulation box is 200λ $(x) \times 120\lambda$ (y), with resolution dx = 0.02λ and dy = 0.08λ . For the 3D simulation, the simulation box is 200λ $(x) \times 50\lambda$ $(y) \times 50\lambda$ (z) for transverse injection and 200λ $(x) \times 70\lambda$ $(y) \times 70\lambda$ (z) for longitudinal injection. The spatial resolution is dx = $\lambda/32$ and dy = dz = 0.1λ . A moving window is used to accelerate the electrons sufficiently, and there are four pseudo-particles per cell for each particle species.

A. Transverse self-injection mechanism

In the case of the transverse self-injection mechanism, the accelerated electrons are initially located at the transverse radii, and the injection process is affected by the distribution of the electromagnetic field, which is determined by the bubble geometry. On the basis of the work of Li *et al.*, 47 the electromagnetic field of an ellipsoidal bubble can be written as

$$E_{x} = \frac{\eta^{2}}{\eta^{2}(1 - v_{b}^{2}) + 2}\xi,$$
 (8a)

$$E_{y} = \frac{2 - \eta^{2} v_{b}^{2}}{2\eta^{2} (1 - v_{b}^{2}) + 4} y,$$
 (8b)

$$E_z = \frac{2 - \eta^2 v_b^2}{2\eta^2 (1 - v_b^2) + 4} z,$$
 (8c)

$$B_x = 0, (8d)$$

$$B_{y} = \frac{v_{b}\eta^{2}}{2\eta^{2}(1 - v_{b}^{2}) + 4}z,$$
 (8e)

$$B_z = -\frac{v_b \eta^2}{2\eta^2 (1 - v_b^2) + 4} y,$$
 (8f)

where $\xi=x-v_bt$, $v_b=\sqrt{1-\gamma_b^{-2}}$ is the bubble phase velocity, and $\gamma_b=0.45\sqrt{n_c/n_0}$. $^{48.49}$ To confine the field distribution inside the bubble, a modified factor $f(r)=[\tanh(R_\parallel/d-r/d)+1]/2$ is used, where $r=\sqrt{\xi^2+(y^2+z^2)/\eta^2}$ and d is the width of the electron sheath. In this work, d=0.5 is adopted. The aspect ratio $\eta=R_\perp/R_\parallel$ is defined to describe the geometry of the bubble, where R_\parallel and R_\perp are the longitudinal and transverse radii, respectively. They are calculated directly through 2D PIC simulation. According to this definition, $\eta<1$, $\eta=1$, and $\eta>1$ indicate a prolate spheroid, a sphere, and an oblate spheroid, respectively.

The electron dynamics in the bubble field are calculated using the fourth-order Runge–Kutta method based on the relativistic Newton–Lorentz equation $d\mathbf{P}/dt = -e[\mathbf{E} + (\mathbf{P}/\gamma) \times \mathbf{B}]$, where $\gamma = 1/\sqrt{1-v^2/c^2}$ is the relativistic factor of the electrons. Meanwhile, the spin precession of an electron is calculated according to the TBMT equation with the Boris-rotation method. The electrons are initially located at the front of the bubble, denoted as (x_0, y_0, z_0) . The initial direction of electron spin s_0 is changed in the xy plane in order to study the effect of initial spin on the final polarization.

The final distributions of electron spin s_{\parallel} with initial transverse position (R_0, φ_0) are presented in Fig. 3, where $R_0 = \sqrt{y_0^2 + z_0^2}$ and $\varphi_0 = \tan^{-1}(z_0/y_0)$. $\theta_0 = \tan^{-1}(s_{0y}/s_{0x})$ denotes the initial spin direction. $\theta_0 = 0^{\circ}$ indicates that the initial spin is aligned with the laser-propagation direction. Electrons with final kinetic energy larger than 20 MeV are selected as the accelerated electrons. It turns out that the accelerated electrons are initially located around the transverse radius, as indicated by the white dashed circles in Fig. 3(a). More importantly, the distribution of s_{\parallel} is axially symmetric. When the initial state of the spin, θ_0 , is changed, there is an obvious difference in the final distribution of s_{\parallel} , and not only for accelerated electrons, as revealed in Figs. 3(b) and 3(c). The distribution of electron spin s_{\parallel} does not obviously change for electrons initially located on the z axis, whereas the value of s_{\parallel} increases from $\theta_0 = 0^{\circ}$ to 90° for electrons initially located on the y axis. As a consequence, the polarization of the accelerated electron beam depends on the initial spin state.

According to the theoretical analysis in Sec. II, the spin precession of the accelerated electrons is determined by Ω_{φ} , which leads to rotation of the electron spin around the direction of $\hat{\varphi}$, as a consequence of which the distribution of s_{\parallel} is isotropic at $\theta_0 = 0^{\circ}$ and anisotropic at $\theta_0 = 45^{\circ}$ and 90° . Furthermore, $\langle s_{\parallel} \rangle$ is independent of the pre-polarization angle θ_0 for electrons located on the z axis, whereas $\langle s_{\parallel} \rangle$ depends on θ_0 for electrons located on the y axis.

This phenomenon can be explained by examining the electron trajectory and spin precession, as shown in Figs. 4(a) and 4(b) for two typical electrons with the same distance from the x axis. The electron spin is initially aligned along the y axis, i.e., $\theta_0 = 90^\circ$, and

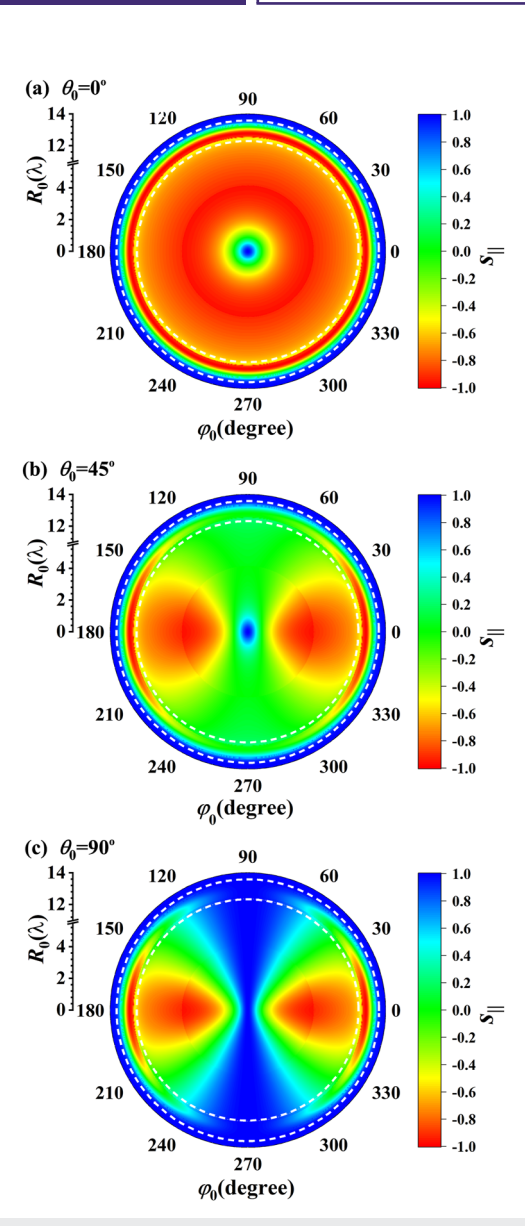
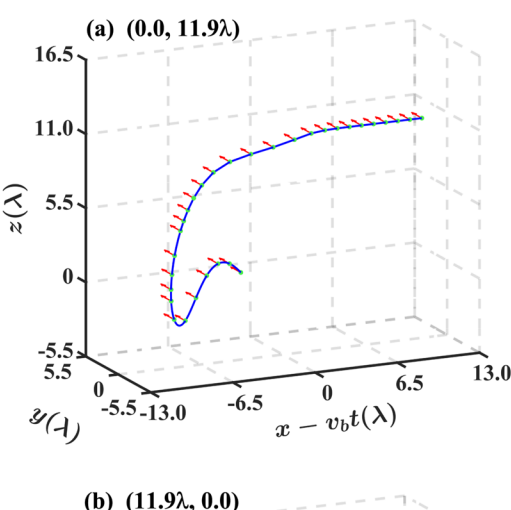


FIG. 3. Distributions of s_{\parallel} as a function of initial electron position (R_0,φ_0) for different initial polarization directions $\theta_0=0^\circ$ (a), 45° (b), and 90° (c). Here, $R_0=\sqrt{y_0^2+z_0^2},\;\varphi_0=\tan^{-1}(z_0/y_0),\;$ and $\theta_0=\tan^{-1}(s_{0y}/s_{0x}).\;$ The laser parameters are $a_0=20,\;w_0=10\lambda,\;$ and $\tau=21$ fs, and the plasma density is $n_0=0.021n_c.\;$ The bubble parameters are obtained through the PIC simulations, where $R_{\parallel}=10.31\lambda,\;R_{\perp}=12.34\lambda,\;$ and $\eta=R_{\perp}/R_{\parallel}=1.20.\;$ The electrons, initially located in the region between the white dashed cicles from R_0 min to $R_{0\text{max}}$, can be captured by the bubble and finally obtain high energy.

the other parameters are the same as those in Fig. 3(c). As can be seen in Fig. 4(a), the spin of the accelerated electron located initially on the z axis does not fluctuate with time, because its spin direction is always aligned with the direction of the precession frequency Ω . On the contrary, as can be seen in Fig. 4(b), for the accelerated electron initially located on the y axis, the spin direction starts to rotate around the z axis. Thus, it is demonstrated that the electron spin



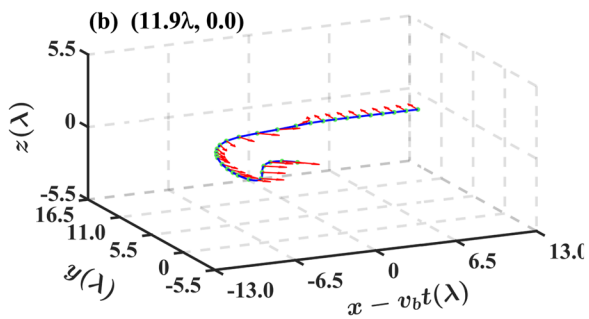


FIG. 4. Evolution of electron trajectory (blue solid lines) and spin precession (red arrows) in the case of transverse injection. The initial electron position (y_0, z_0) is $(0.0, 11.9\lambda)$ and $(11.9\lambda, 0.0)$ in [(a) and (b)], respectively. The other parameters are same as those in Fig. 3(c).

is mainly influenced by Ω_z , which is consistent with the theoretical analysis.

The net polarization of a particle beam is defined as $P = \sqrt{\langle s_x \rangle^2 + \langle s_y \rangle^2 + \langle s_z \rangle^2}$, where $\langle s_i \rangle$ are the average values in each direction. Figure 5(a) compares $\langle s_\parallel \rangle$ of accelerated electrons obtained from 3D PIC simulation, theoretical analysis [Eq. (6)], and test particle dynamics simulation. Here, the first bunch of accelerated electron beams is chosen, whose kinetic energy $E_k > 100$ MeV at 500 fs in the 3D PIC simulation, in order to minimize the effect of bubble evolution caused by the laser evolution and electron acceleration. The $\langle s_\parallel \rangle$ of the electron beam increases with increasing θ_0 . The results from the test particle dynamics simulation are in agreement with those from the theoretical analysis. Here, $\langle \cos \alpha_r \rangle$ is chosen on the basis of the test particle dynamics results. However, there is a tiny difference between the theoretical results and those from the 3D PIC simulation, owing to limitations of the theoretical model of the bubble field. ⁵⁰

For the 2D PIC simulation, Figs. 5(b) and 5(c) show the effect of θ_0 on the polarization of the accelerated electron beam $\langle s_{\parallel} \rangle$ in the xy ($\varphi = 0^{\circ}$ or 180°) and xz planes ($\varphi = \pm 90^{\circ}$), respectively. When the simulation box is located in the xy plane [Fig. 5(b)], the evolution of $\langle s_{\parallel} \rangle$ is independent of the initial spin state, because the spin precession axis is always perpendicular to the instantaneous electron

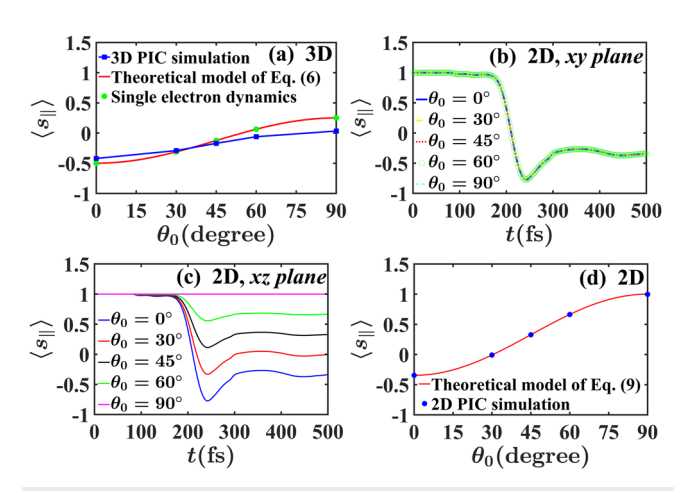


FIG. 5. (a) Relationship between the polarization $\langle s_{\parallel} \rangle$ of the accelerated electron beam and the pre-polarization angle θ_0 , obtained from 3D PIC simulation, theoretical analysis [Eq. (6)], and test particle dynamics simulation. Here, the electrons with $E_k > 100$ MeV at 500 fs are chosen as accelerated electrons. [(b) and (c)] Evolution of $\langle s_{\parallel} \rangle$ about the electron beam for different pre-polarization angles θ_0 from 2D PIC simulations in the xy and xz planes, respectively. (d) Distribution of $\langle s_{\parallel} \rangle$ with θ_0 for the accelerated electrons from 2D PIC simulation in the xz plane and from the theoretical model [Eq. (9)]. The accelerated electrons are chosen on the basis of their position and energy in the 2D case, where $105.0\lambda < x < 108.0\lambda$, $|y| < 1.4\lambda$ (or $|z| < 1.4\lambda$), and $E_k > 35$ MeV at 360 fs on the xy (or xz) planes. The laser parameters are $a_0 = 20$, $w_0 = 10\lambda$, and $\tau = 21$ fs. The plasma density is $n_0 = 0.021n_c$ and $L_1 = 10\lambda$.

spin direction. According to Eq. (5) and assuming $\beta_0 = 0^\circ$, the electron spin can be written as $s_{\parallel} = \cos \alpha_r$, which means that the electron spin is independent of the initial spin orientation.

When the simulation box is located in the xz plane, the polarization dynamics is affected by the initial state, as revealed in Fig. 5(c). On the basis of Eq. (5) and assuming $\beta_0 = 0^\circ$, the electron spin can be written as $s_{\parallel} = \cos \alpha_r + 2 \sin^2 (\alpha_r/2) \sin^2 \theta_0$. The polarization of the accelerated electrons is then obtained as

$$\begin{aligned} \langle s_{\parallel} \rangle &= \frac{\int_{z_{\text{0min}}}^{z_{\text{0min}}} s_{\parallel} \, \mathrm{d}z}{\int_{z_{\text{0min}}}^{z_{\text{0max}}} \, \mathrm{d}z} \\ &= \langle \cos \alpha_{r} \rangle (1 - \sin^{2} \theta_{0}) + \sin^{2} \theta_{0}, \end{aligned} \tag{9}$$

where $\langle \cos \alpha_r \rangle = \int_{z_{0\,\text{min}}}^{z_{0\,\text{max}}} \cos \alpha_r \, \mathrm{d}z / (z_{0\,\text{max}} - z_{0\,\text{min}})$. Here, it is assumed that electrons with initial position from $z_{0\,\text{min}}$ to $z_{0\,\text{max}}$ are injected into the bubble. The 2D theoretical model is in agreement with the 2D PIC simulations, as shown in Fig. 5(d).

In the above discussion, a phenomenological model has been used to describe the properties of the bubble geometry and field, since this is an efficient approach for the study of test particle dynamics. Lu *et al.*⁵¹ proposed an equation for the bubble boundary, and further developments in theoretical models^{50,52–57} have provided descriptions of the bubble regime that give more accurate fits with numerical simulations. Most of these theoretical developments have focused on particle-driven wakefield acceleration, since the evolution of the driver can be ignored and it can be directly described using its initial profile. However, for LWFA, the evolution

of the laser is a 3D nonlinear phenomenon, and it is therefore difficult to accurately describe the laser profile at a given single point, as a consequence of which theoretical models of bubble structure are valid only for the rear half of the bubble regime. 55 Studies of test particle dynamics using the equation for the bubble boundary require more complicated numerical calculations of the electromagnetic field at each time step, and the final results still disagree slightly with those of PIC simulations. Fortunately, in the case of transverse self-injection, the injection process occurs mainly in the rear half of the bubble regime, and the distribution of the bubble field does not depart from axial symmetry, which means that the theoretical description of the effect of initial spin orientation retains its validity.

B. Longitudinal self-injection mechanism

For longitudinal injection in the quasi-1D regime, the electron spin is mainly affected by the laser field, according to Ref. 41. Because the laser evolution in the plasma is a nonlinear phenomenon, it is difficult to derive an appropriate expression for the laser field. In addition, the laser profile does not vary significantly during the interaction with the injected electrons. It is therefore reasonable to consider the effects of the electron–laser interaction in vacuum. The electric field of the laser in the y direction is given by Eq. (7). The other electric and magnetic field components can be obtained using $E_x = (i/k_0)(\partial E_y/\partial y)$, $B = -(i/\omega_0)\nabla \times E$ in the paraxial approximation. Since S_0 Similar to the case of the bubble fields, the electrons are at rest in front of the laser field at a position S_0 , S_0 , and their spins S_0 are initially located in the S_0 Plane, i.e., S_0 of S_0 . The laser parameters are S_0 and S_0 and S_0 and S_0 are initially located in the S_0 Plane, i.e., S_0 of S_0 . The laser parameters are S_0 and S_0 and S_0 and S_0 are initially located in the S_0 plane, i.e.,

The final s_{\parallel} distributions at t = 300 fs of electrons with initial positions (y_0, z_0) and initial spin directions $\theta_0 = 0^{\circ}$, 45° , and 90° are shown in Figs. 6(b)-6(d), respectively. The spins of electrons that are initially near the laser axis remain nearly unchanged after

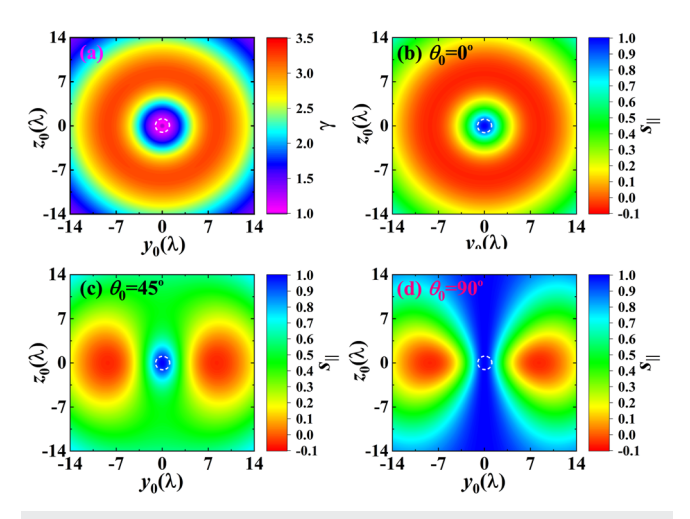


FIG. 6. (a) Distribution of final energy γ of electrons with initial positions (y_0,z_0) after interacting with the laser in vacuum, according to the test particle dynamics simulation. [(b)–(d)] Distributions of s_{\parallel} of electrons with initial positions (y_0,z_0) and initial polarization directions $\theta_0=0^\circ,45^\circ,$ and $90^\circ,$ respectively. The laser parameters are $a_0=6$, $w_0=20\lambda,$ and $\tau=17$ fs. The initial positions of electrons within $r_0=\pm\lambda$ are marked by the white circles.

interaction with the laser pulse, as indicated by the white circles. During the longitudinal injection process, the trajectories of the accelerated electrons are close to the laser axis, as a consequence of which the net depolarization effect is almost zero, even though the laser field can cause some spin precession of the electrons. When the electrons reach the tail of the bubble, the influence of the bubble field on spin precession can also be ignored, because the transverse electromagnetic field and the transverse velocity of the electrons are very small.⁴¹

With increasing distance from the electron initial position to the laser axis, the situation clearly changes, as depicted in Fig. 6. The distribution of electron energy is axially symmetric, as revealed in Fig. 6(a), and the electron dynamics can be explained by the ponderomotive potential model. The transverse and longitudinal ponderomotive forces induced by the laser propagating along the x axis can be derived as F_r and F_x . The transverse ponderomotive force is almost off-axis and the electron is always expelled transversely, while the longitudinal ponderomotive force is basically positive and hence accelerates the electron longitudinally. Thus, the electrons have a transverse velocity \widetilde{v}_r and a longitudinal velocity \widetilde{v}_x . The equivalent transverse (\widetilde{E}_r) and longitudinal (\widetilde{E}_x) electric fields are defined on the basis of the ponderomotive model. More importantly, the electron velocity \widetilde{v}_φ is zero, and the equivalent electric field \widetilde{E}_φ is also zero.

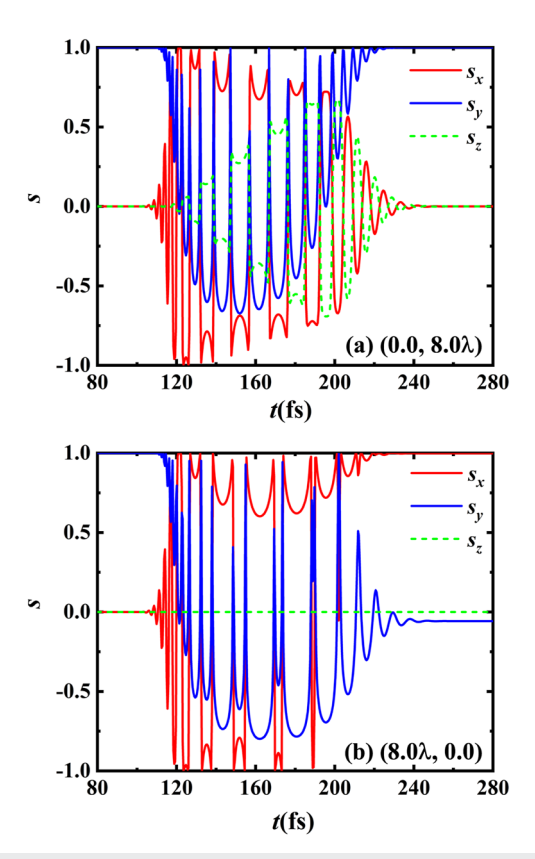


FIG. 7. Evolution of electron spin in each direction for typical electrons with initial positions $(y_0, z_0) = (0.0, 8.0\lambda)$ (a) and $(8.0\lambda, 0.0)$ (b). The laser parameters and initial spin state are the same as in Fig. 6(d).

During the interaction between the laser and the electrons, the electrons gain net energy, and their spins change simultaneously. According to the TBMT equation, $\Omega \propto \widetilde{\boldsymbol{v}} \times \widetilde{\boldsymbol{E}}$, and it can be derived that $\Omega = \widetilde{\Omega}_{\varphi}$. Therefore, the distribution of electron spin is axially symmetric in the case of $\theta_0 = 0^\circ$, as observed in Fig. 6(b). When the initial spin direction is changed, the final distribution of electron spin is also altered, which is similar to the case of the bubble field, as illustrated in Figs. 6(c) and 6(d).

To confirm the results of the theoretical analysis, the spin evolution of two electrons with typical initial positions is presented in Fig. 7. Here, the initial electron spin is aligned with the y axis. The other parameters are same as those in Fig. 6(d). For an electron initially located on the z axis, the spin direction is always parallel to the precession frequency $\widetilde{\Omega}_{\varphi}$. Then, s_y quivers in the laser field, while the net depolarization is zero, as demonstrated in Fig. 7(a). An electron initially located on the y axis oscillates in the xy plane under the action of the laser field, with its spin always perpendicular to the precession frequency $\widetilde{\Omega}_{\varphi}$, and hence s_z is always zero, as shown in Fig. 7(b).

Figure 8 displays the related results of PIC simulation. Here, the initial laser amplitude is $a_0 = 6$, the laser waist is $w_0 = 20\lambda$, the laser pulse duration is $\tau = 17$ fs, the length of the up-ramp transition is $L_1 = 45\lambda$, the density of the plateau is $n_0 = 0.04n_c$, and the other parameters are same as those in the case of transverse injection. Electrons with energy larger than 35 MeV at 360 fs are chosen as the accelerated electrons for the longitudinal injection process in the 2D case. As shown in Figs. 8(a) and 8(b), the 2D simulation results confirm those of the theoretical analysis based on the ponderomotive model. The effect of initial spin orientation can be ignored at the final time. While the electrons interact with the laser, the electron spin is affected by the laser directly at around 200 fs.

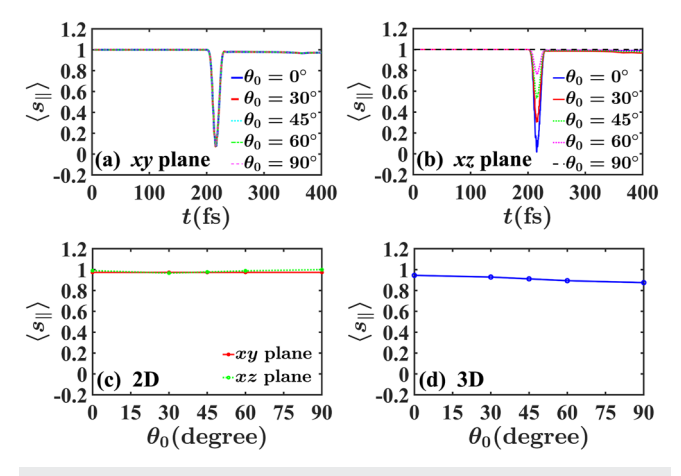


FIG. 8. [(a) and (b)] Evolution of polarization $\langle s_\parallel \rangle$ for accelerated electrons in the longitudinal injection case with different pre-polarization angles θ_0 from 2D PIC simulations in the xy and xz planes, respectively. Electrons with 146.0 $\lambda < x < 147.0\lambda$, $|y| < 5\lambda$ (or $|z| < 5\lambda$) and $E_k > 35$ MeV at 360 fs are selected in the 2D case in the xy (or xz) plane. [(c) and (d)] Relationship between initial spin direction θ_0 and $\langle s_\parallel \rangle$ of accelerated electrons from 2D and 3D PIC simulations, respectively. Electrons with $E_k > 100$ MeV at 500 fs are chosen as accelerated electrons in the 3D PIC simulation. Here, the laser parameters are $a_0 = 6$, $w_0 = 20\lambda$. and $\tau = 17$ fs. and the plasma density is $n_0 = 0.040n_c$ and $L_1 = 45\lambda$.

The electrons do not gain net energy after interacting with the laser, and the net depolarization effect is nearly zero for the longitudinal injection scheme, as presented in Figs. 8(c) and 8(d). Compared with the case of transverse injection, longitudinal injection is more stable in providing an electron beam with high polarization, and, in particular, independent of the direction of initial spin.

IV. CONCLUSION

The effect of initial spin orientation on the polarization of accelerated electrons in the LWFA regime has been investigated theoretically and numerically using the Thomas-Bargmann-Michel-Telegdi equation. It has been found that the final spin polarization is dependent upon the self-injection process, i.e., whether this is transverse or longitudinal self-injection. In the case of transverse injection, the electron spin is mainly affected by the bubble field, and the direction of the precession frequency is fixed in the vertical plane of the electron trajectory. The spins of several electrons do not move when their spins are initially aligned with the direction of precession frequency, and consequently the final polarization of the accelerated electron beam to depend on its initial spin orientation. However, in the case of longitudinal injection, the dynamics of electron spin are mainly determined by the laser field. Because the net effect of the laser field is negligible, the polarization of the accelerated electrons is independent of their initial spin status. The results of 3D PIC simulation are consistent with those from test particle dynamics simulation and theoretical analysis. This study indicates that the longitudinal self-injection mechanism exhibits more stability in obtaining a bunch of electrons with high polarization, compared with transverse self-injection. Furthermore, the present investigation of the effects of bubble and laser fields on electron spin should provide useful guidance for studies of polarization dynamics in other acceleration schemes.

ACKNOWLEDGMENTS

This work was supported by the National Natural Science Foundation of China (Grant Nos. 11804348, 11775056, 11975154, 12225505, and 12405281) and the Science Challenge (Project No. TZ2018005). X. F. Li was also supported by the Shanghai Pujiang Program (Grant No. 23PJ1414600) and the Strategic Priority Research Program of the Chinese Academy of Sciences (Grant No. XDB0890203). The work of M. Büscher was carried out in the framework of the Jülich Short-Pulse Particle and Radiation Center and was supported by the Accelerator Technology Helmholtz Infrastructure consortium ATHENA. We thank M. Zeng and Y. L. Liu for helpful discussions about the theoretical model of particle-driven wakefield acceleration.

AUTHOR DECLARATIONS

Conflict of Interest

The authors have no conflicts to disclose.

Author Contributions

X. F. Li and Q. Kong proposed the idea, supervised the work, and improved the manuscript. L. R. Yin developed the theoretical

model, carried out all simulations, analyzed the results, and drafted the manuscript. X. F. Li, Y. J. Gu, N. Cao, M. Büscher, S. M. Weng, M. Chen, and Z. M. Sheng improved the manuscript. All authors discussed the results, commented on the manuscript, and agreed on the contents.

L. R. Yin: Data curation (equal); Formal analysis (equal); Investigation (equal); Validation (equal); Visualization (equal); Writing – review original draft (equal). X. F. Li: Conceptualization (equal); Project administration (equal); Software (equal); Supervision (equal); Writing – review review & editing (equal). Y. J. Gu: Writing – review review & editing (equal). N. Cao: Writing – review review & editing (equal); Supervision (equal); Writing – review review & editing (equal). M. Büscher: Writing – review review & editing (equal). S. M. Weng: Writing – review review & editing (equal). M. Chen: Writing – review review & editing (equal). Z. M. Sheng: Writing – review review & editing (equal).

DATA AVAILABILITY

The data that support the findings of this study are available from the corresponding author upon reasonable request.

REFERENCES

- ¹C. Glashausser, "Nuclear physics with polarized beams," Annu. Rev. Nucl. Part. Sci. **29**, 33 (1979).
- ²D. Androić, D. S. Armstrong, A. Asaturyan, T. Averett, J. Balewski *et al.*, "Precision measurement of the weak charge of the proton," Nature 557, 207 (2018)
- ³G. Moortgat-Pick, T. Abe, G. Alexander, B. Anantha-narayan, A. A. Babich *et al.*, "Polarized positrons and electrons at the linear collider," Phys. Rep. **460**, 131 (2008).
- ⁴M. Burkardt, C. A. Miller, and W. D. Nowak, "Spin-polarized high-energy scattering of charged leptons on nucleons," Rep. Prog. Phys. **73**, 016201 (2010).
- ⁵E. S. Ageev, V. Y. Alexakhin, Y. Alexandrov, G. D. Alexeev, A. Amoroso *et al.*, "Measurement of the spin structure of the deuteron in the DIS region," Phys. Lett. B **612**, 154 (2005).
- ⁶R. Märtin, G. Weber, R. Barday, Y. Fritzsche, U. Spillmann *et al.*, "Polarization transfer of bremsstrahlung arising from spin-polarized electrons," Phys. Rev. Lett. **108**, 264801 (2012).
- ⁷D. Abbott, P. Adderley, A. Adeyemi, P. Aguilera, M. Ali *et al.*, "Production of highly polarized positrons using polarized electrons at MeV energies," Phys. Rev. Lett. **116**, 214801 (2016).
- ⁸ K. Xue, Z. K. Dou, F. Wan, T. P. Yu, W. M. Wang *et al.*, "Generation of highly-polarized high-energy brilliant *y*-rays via laser-plasma interaction," Matter Radiat. Extremes **5**, 054402 (2020).
- ⁹S. Tang, Y. Xin, M. Wen, M. A. Bake, and B. Xie, "Fully polarized Compton scattering in plane waves and its polarization transfer," Matter Radiat. Extremes 9, 037204 (2024).
- ¹⁰Z. W. Lu, X. D. Hou, F. Wan, Y. I. Salamin, C. Lv et al., "Diagnosis of ultrafast ultraintense laser pulse characteristics by machine-learning-assisted electron spin," Matter Radiat. Extremes 8, 034401 (2023).
- ¹¹ A. A. Sokolov and I. M. Ternov, "Synchrotron radiation," Sov. Phys. J. **10**, 39 (1967).
- ¹²S. R. Mane, Y. M. Shatunov, and K. Yokoya, "Spin-polarized charged particle beams in high-energy accelerators," Rep. Prog. Phys. 68, 1997 (2005).
- ¹³ M. Chodorow, E. L. Ginzton, W. W. Hansen, R. L. Kyhl, R. B. Neal *et al.*, "Stanford high-energy linear electron accelerator (Mark III)," Rev. Sci. Instrum. 26, 134 (1955).

- ¹⁴H. Wiedemann, Particle Accelerator Physics (Springer Nature, 2015).
- ¹⁵T. Tajima and J. M. Dawson, "Laser electron accelerator," Phys. Rev. Lett. 43, 267 (1979).
- ¹⁶E. Esarey, C. B. Schroeder, and W. P. Leemans, "Physics of laser-driven plasma-based electron accelerators," Rev. Mod. Phys. 81, 1229 (2009).
- ¹⁷C. G. R. Geddes, C. Toth, J. Van Tilborg, E. Esarey, C. B. Schroeder *et al.*, "High-quality electron beams from a laser wakefield accelerator using plasma-channel guiding," Nature **431**, 538 (2004).
- ¹⁸X. Wang, R. Zgadzaj, N. Fazel, Z. Li, S. A. Yi *et al.*, "Quasi-monoenergetic laser-plasma acceleration of electrons to 2 GeV," Nat. Commun. 4, 1988 (2013).
- ¹⁹J. Osterhoff, A. Popp, Z. Major, B. Marx, T. P. Rowlands-Rees *et al.*, "Generation of stable, low-divergence electron beams by laser-wakefield acceleration in a steady-state-flow gas cell," Phys. Rev. Lett. **101**, 085002 (2008).
- ²⁰E. Brunetti, R. P. Shanks, G. G. Manahan, M. R. Islam, B. Ersfeld *et al.*, "Low emittance, high brilliance relativistic electron beams from a laser-plasma accelerator," Phys. Rev. Lett. **105**, 215007 (2010).
- ²¹ W. P. Leemans, B. Nagler, A. J. Gonsalves, C. Tóth, K. Nakamura *et al.*, "GeV electron beams from a centimetre-scale accelerator," Nat. Phys. **2**, 696 (2006).
- ²² A. J. Gonsalves, K. Nakamura, J. Daniels, C. Benedetti, C. Pieronek *et al.*, "Petawatt laser guiding and electron beam acceleration to 8 GeV in a laser-heated capillary discharge waveguide," Phys. Rev. Lett. 122, 084801 (2019).
- ²³ J. Wang, M. Zeng, D. Li, X. Wang, W. Lu *et al.*, "Injection induced by coaxial laser interference in laser wakefield accelerators," Matter Radiat. Extremes 7, 054001 (2022).
- ²⁴ A. Picksley, J. Chappell, E. Archer, N. Bourgeois, J. Cowley *et al.*, "All-optical GeV electron bunch generation in a laser-plasma accelerator via truncated-channel injection," Phys. Rev. Lett. 131, 245001 (2023).
- ²⁵Z. Xiang, C. Yu, Z. Qin, X. Jiao, J. Cheng *et al.*, "Ultrahigh-brightness 50 MeV electron beam generation from laser wakefield acceleration in a weakly nonlinear regime," Matter Radiat. Extremes **9**, 035201 (2024).
- ²⁶D. Sofikitis, P. Glodic, G. Koumarianou, H. Jiang, L. Bougas *et al.*, "Highly nuclear-spin-polarized deuterium atoms from the UV photodissociation of deuterium iodide," Phys. Rev. Lett. **118**, 233401 (2017).
- ²⁷D. Sofikitis, C. S. Kannis, G. K. Boulogiannis, and T. P. Rakitzis, "Ultrahigh-density spin-polarized H and D observed via magnetization quantum beats," Phys. Rev. Lett. 121, 083001 (2018).
- ²⁸ M. Wen, M. Tamburini, and C. H. Keitel, "Polarized laser-wakefield-accelerated kiloampere electron beams," Phys. Rev. Lett. **122**, 214801 (2019).
- ²⁹Y. Wu, L. Ji, X. Geng, Q. Yu, N. Wang *et al.*, "Polarized electron-beam acceleration driven by vortex laser pulses," New J. Phys. **21**, 073052 (2019).
- ³⁰Y. Wu, L. Ji, X. Geng, Q. Yu, N. Wang *et al.*, "Polarized electron acceleration in beam-driven plasma wakefield based on density down-ramp injection," Phys. Rev. E **100**, 043202 (2019).
- ³¹Y. Wu, L. Ji, X. Geng, J. Thomas, M. Büscher *et al.*, "Spin filter for polarized electron acceleration in plasma wakefields," Phys. Rev. Appl. **13**, 044064 (2020).
- ³²Z. Nie, F. Li, F. Morales, S. Patchkovskii, O. Smirnova *et al.*, "*In situ* generation of high-energy spin-polarized electrons in a beam-driven plasma wakefield accelerator," Phys. Rev. Lett. **126**, 054801 (2021).
- ³³Z. Nie, F. Li, F. Morales, S. Patchkovskii, O. Smirnova *et al.*, "Highly spin-polarized multi-GeV electron beams generated by single-species plasma photocathodes," Phys. Rev. Res. 4, 033015 (2022).
- ³⁴T. Sun, Q. Zhao, F. Wan, Y. I. Salamin, and J. X. Li, "Generation of ultrabrilliant polarized attosecond electron bunches via dual-wake injection," Phys. Rev. Lett. 132, 045001 (2024).
- ³⁵Z. Gong, M. J. Quin, S. Bohlen, C. H. Keitel, K. Póder *et al.*, "Spin-polarized electron beam generation in the colliding-pulse injection scheme," Matter Radiat. Extremes **8**, 064005 (2023).
- ³⁶S. Bohlen, Z. Gong, M. J. Quin, M. Tamburini, and K. Pöder, "Colliding pulse injection of polarized electron bunches in a laser-plasma accelerator," Phys. Rev. Res. 5, 033205 (2023).
- ³⁷S. Corde, C. Thaury, A. Lifschitz, G. Lambert, K. Ta Phuoc *et al.*, "Observation of longitudinal and transverse self-injections in laser-plasma accelerators," Nat. Commun. **4**, 1501 (2013).

- ³⁸I. Kostyukov, E. Nerush, A. Pukhov, and V. Seredov, "Electron self-injection in multidimensional relativistic-plasma wake fields," Phys. Rev. Lett. **103**, 175003 (2009).
- ³⁹ H. C. Fan, X. Y. Liu, X. F. Li, J. F. Qu, Q. Yu *et al.*, "Control of electron beam polarization in the bubble regime of laser-wakefield acceleration," New J. Phys. **24**, 083047 (2022).
- ⁴⁰F. Y. Li, Z. M. Sheng, Y. Liu, J. Meyer-ter-Vehn, W. B. Mori *et al.*, "Dense attosecond electron sheets from laser wakefields using an up-ramp density transition," Phys. Rev. Lett. **110**, 135002 (2013).
- ⁴¹ L. R. Yin, X. F. Li, Y. J. Gu, N. Cao, Q. Kong *et al.*, "Generation of polarized electron beams through self-injection in the interaction of a laser with a pre-polarized plasma," High Power Laser Sci. Eng. 12, e28 (2024).
- ⁴²M. Büscher, A. Hützen, L. Ji, and A. Lehrach, "Generation of polarized particle beams at relativistic laser intensities," High Power Laser Sci. Eng. **8**, e36 (2020)
- ⁴³L. H. Thomas, "The Motion of the spinning electron," Nature 117, 514 (1926).
- ⁴⁴J. Thomas, A. Hützen, A. Lehrach, A. Pukhov, L. Ji *et al.*, "Scaling laws for the depolarization time of relativistic particle beams in strong fields," Phys. Rev. Accel. Beams **23**, 064401 (2020).
- ⁴⁵T. D. Arber, K. Bennett, C. S. Brady, A. LawrenceDouglas, M. G. Ramsay *et al.*, "Contemporary particle-in-cell approach to laser-plasma modelling," Plasma Phys. Control. Fusion **57**, 113001 (2015).
- ⁴⁶X. F. Li, P. Gibbon, A. Hützen, M. Büscher, S. M. Weng *et al.*, "Polarized proton acceleration in ultraintense laser interaction with near-critical-density plasmas," Phys. Rev. E **104**, 015216 (2021).
- ⁴⁷X. F. Li, Q. Yu, Y. J. Gu, S. Huang, Q. Kong *et al.*, "Bubble shape and electromagnetic field in the nonlinear regime for laser wakefield acceleration," Phys. Plasmas **22**, 083112 (2015).
- ⁴⁸I. Kostyukov, A. Pukhov, and S. Kiselev, "Phenomenological theory of laser-plasma interaction in 'bubble' regime," Phys. Plasmas 11, 5256 (2004).
- ⁴⁹C. B. Schroeder, C. Benedetti, E. Esarey, and W. P. Leemans, "Nonlinear pulse propagation and phase velocity of laser-driven plasma waves," Phys. Rev. Lett. **106**, 135002 (2011).

- ⁵⁰ A. Golovanov, I. Y. Kostyukov, A. Pukhov, and V. Malka, "Energy-conserving theory of the blowout regime of plasma wakefield," Phys. Rev. Lett. 130, 105001 (2023).
- ⁵¹W. Lu, C. Huang, M. Zhou, M. Tzoufras, F. S. Tsung *et al.*, "A nonlinear theory for multidimensional relativistic plasma wave wakefields," Phys. Plasmas **13**, 056709 (2006).
- ⁵²S. A. Yi, V. Khudik, C. Siemon, and G. Shvets, "Analytic model of electromagnetic fields around a plasma bubble in the blow-out regime," Phys. Plasmas 20, 013108 (2013).
- ⁵³J. Thomas, I. Y. Kostyukov, J. Pronold, A. Golovanov, and A. Pukhov, "Non-linear theory of a cavitated plasma wake in a plasma channel for special applications and control," Phys. Plasmas 23, 053108 (2016).
- ⁵⁴A. A. Golovanov, I. Y. Kostyukov, J. Thomas, and A. Pukhov, "Analytic model for electromagnetic fields in the bubble regime of plasma wakefield in non-uniform plasmas," Phys. Plasmas 24, 103104 (2017).
- ⁵⁵T. N. Dalichaouch, X. L. Xu, A. Tableman, F. Li, F. S. Tsung *et al.*, "A multisheath model for highly nonlinear plasma wakefields," Phys. Plasmas **28**, 063103 (2021).
- ⁵⁶A. A. Golovanov, I. Y. Kostyukov, L. Reichwein, J. Thomas, and A. Pukhov, "Excitation of strongly nonlinear plasma wakefield by electron bunches," Plasma Phys. Control. Fusion 63, 085004 (2021).
- ⁵⁷Y. Liu, M. Zeng, L. Reichwein, and A. Pukhov, "Adiabatic sheath model for beam-driven blowout plasma channels," Phys. Rev. Res. 7, 023101 (2025).
- ⁵⁸ P. X. Wang, Y. K. Ho, X. Q. Yuan, Q. Kong, N. Cao et al., "Characteristics of laser-driven electron acceleration in vacuum," J. Appl. Phys. 91, 856–866 (2002).
- ⁵⁹Q. Kong, S. Miyazaki, S. Kawata, K. Miyauchi, K. Nakajima *et al.*, "Electron bunch acceleration and trapping by the ponderomotive force of an intense short-pulse laser," Phys. Plasmas **10**, 4605 (2003).
- ⁶⁰ D. Lin, Q. Kong, Z. Chen, P. X. Wang, and Y. K. Ho, "Characteristics of electron ponderomotive acceleration by a laser pulse in vacuum," J. Phys. D: Appl. Phys. **41**, 135107 (2008).
- ⁶¹ M. Büscher, R. Adam, C. Tusche, A. Hützen, C. Wiemann *et al.*, "JuSPARC-The Jülich short-pulsed particle and radiation center," J. Large-scale Res. Fac. 6, A138 (2020).